

---

# OPTIMIZING MULTI-MODAL MODELS FOR IMAGE-BASED SHAPE RETRIEVAL: THE ROLE OF PRE-ALIGNMENT AND HARD CONTRASTIVE LEARNING

---

**Paul Julius Kühn** 

Fraunhofer IGD, 64283 Darmstadt, Germany

**Cedric Spengler** 

Fraunhofer IGD, 64283 Darmstadt, Germany

**Michael Weinmann** 

Delft University of Technology, 2628 CD Delft, Netherlands

**Arjan Kuijper** 

Fraunhofer IGD, 64283 Darmstadt, Germany

**Saptarshi Neil Sinha** 

Fraunhofer IGD, 64283 Darmstadt, Germany

## ABSTRACT

Image-based shape retrieval (IBSR) aims to retrieve 3D models from a database given a query image, hence addressing a classical task in computer vision, computer graphics and robotics. Recent approaches typically rely on bridging the domain gap between 2D images and 3D shapes based on the use multi-view renderings as well as task-specific metric learning to embed shapes and images into a common latent space. In contrast, we address IBSR through large-scale multi-modal pretraining and show that explicit view-based supervision is not required. Inspired by pre-aligned image–point-cloud encoders from ULIP and OpenShape that have been used for tasks such as 3D shape classification, we propose the use of pre-aligned image and shape encoders for zero-shot and standard IBSR by embedding images and point clouds into a shared representation space and performing retrieval via similarity search over compact single-embedding shape descriptors. This formulation allows skipping view synthesis and naturally enables zero-shot and cross-domain retrieval without retraining on the target database. We evaluate pre-aligned encoders in both zero-shot and supervised IBSR settings and additionally introduce a multi-modal hard contrastive loss (HCL) to further increase retrieval performance. Our evaluation demonstrates state-of-the-art performance, outperforming related methods on  $Acc_{Top1}$  and  $Acc_{Top10}$  for shape retrieval across multiple datasets, with best results observed for OpenShape combined with Point-BERT. Furthermore, training on our proposed multi-modal HCL yields dataset-dependent gains in standard instance retrieval tasks on shape-centric data, underscoring the value of pretraining and hard contrastive learning for 3D shape retrieval. The code will be made available via the project website.

**Keywords** Image-based shape retrieval · Visual search · Deep learning · Hard contrastive learning

## 1 Introduction

Retrieving 3D shapes from visual observations is a fundamental problem in computer vision with applications in various sectors like e-commerce, inventory management, medical imaging, robotics, cultural heritage and many others. Given a query image, image-based shape retrieval (IBSR) aims to identify the corresponding 3D shape from a database—either at the instance level, recovering the exact depicted object, or at the class level, retrieving any shape of the same semantic category. IBSR requires bridging a fundamental domain gap between 2D images and 3D geometry. This entails two core components: extracting discriminative features from both modalities, and aligning these representations in a shared embedding space where semantically similar image-shape pairs lie close together. The dominant paradigm addresses this challenge by representing 3D shapes as collections of rendered 2D views [39, 11, 10, 17], enabling direct

reuse of image encoders for both modalities. While effective, this approach discards native 3D geometric information and requires rendering shapes from multiple viewpoints at inference time that may not capture all relevant details depending on number and configuration of views. Recent advances in vision-language pre-training offer an alternative path. CLIP [35] demonstrated that contrastive learning on large-scale image-text pairs yields aligned representations enabling zero-shot transfer to diverse downstream tasks. Subsequent work extends this paradigm to 3D: ULIP [48], ULIP-2[49] and OpenShape [26] train point cloud encoders to align with CLIP’s [35] pre-aligned embedding space that allow optimization of these two modalities using deep metric learning, achieving state-of-the-art performance on zero-shot 3D classification. By learning from image-text-point cloud triplets, these models produce geometry-preserving multi-modal representations with strong 3D classification performance. However, their effectiveness for IBSR—particularly zero-shot retrieval and retrieval-specific fine-tuning—remains unexplored. We propose a novel IBSR approach using pre-aligned multimodal encoders that operates directly on point clouds instead of multi-view renderings, eliminating view synthesis dependencies. Additionally, we introduce a multi-modal hard contrastive loss (HCL) that incorporates hard negative sampling for more effective differentiation between similar instances. While hard negative sampling has proven effective in single-modality self-supervised learning [36, 10], its application to IBSR is non-trivial due to the fundamental domain gap between 2D pixels and 3D points. Our novelty lies in adapting this objective to an asymmetric multi-modal setting, where the loss must simultaneously account for hard negatives in two distinct embedding distributions—image negatives for shape anchors and vice versa—to bridge the synthetic-to-real domain shift. To the best of our knowledge, we are the first to apply pre-aligned multi-modal encoders and hard contrastive learning to IBSR, enabling robust cross-dataset retrieval with minimal retraining. We systematically evaluate pre-aligned encoders for IBSR under zero-shot and fine-tuned settings (Fig. 1). We also adapt hard negative mining [36] to the asymmetric image–shape setting via a multi-modal hard contrastive loss (HCL). Rather than proposing a new architecture, we quantify when pre-alignment and hard negatives improve retrieval in practice. In light of these changes the main contributions are:

- We employ and evaluate pre-aligned image and shape encoders for zero-shot and standard IBSR, extending pretraining/alignment techniques from classification to retrieval tasks and avoiding the need for multi-view rendering with its dependence on view selection and density.
- We propose a novel hard contrastive learning method for IBSR tasks, incorporating hard negative sampling to strengthen the model’s discriminative capabilities, enabling better differentiation between similar instances.
- We perform quantitative analysis and ablation studies, demonstrating that the proposed method outperforms prior methods across several benchmarks [46, 41, 50, 21] with  $Acc_{Top10}$  and  $Acc_{Top1}$  performance approaching saturation (reaching  $\approx 100\%$ ). Our proposed HCL improves standard retrieval, particularly for Point-BERT [53] models.

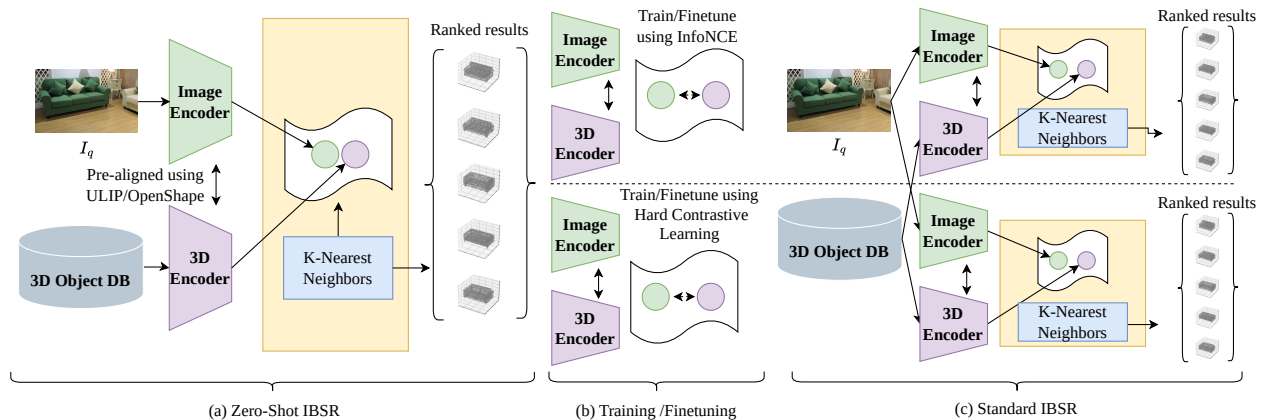


Figure 1: Training pipeline with multiple modalities. Zero-shot retrieval (a) uses pre-aligned image- and shape-encoders trained with multi-modal contrastive losses[48][49][26]. Training or fine-tuning (b) of image- and shape-encoders using either InfoNCE or hard contrastive learning enables standard retrieval (c)

## 2 Related Work

Connecting images to 3D shape repositories spans robotics, AR, and content creation. We review view-based, direct 3D, and multi-modal approaches.

**Multi-View Shape Representations.** The dominant paradigm represents 3D shapes through multiple rendered views. MVCNN [39] pioneered this direction by aggregating CNN features across viewpoints. Follow-up work explores view selection strategies [22], sequential view modeling [18], and hard example mining [10]. These methods typically employ metric learning to align rendered views with query images in a shared embedding space. Notably, by projecting shapes into the 2D domain prior to encoding, such approaches sidestep the challenge of learning directly from 3D geometry—limitation we address in this work. Subsequent methods refine view aggregation through hierarchical grouping [9], joint viewpoint-category learning [20], graph-based view relation modeling [44], and differentiable viewpoint selection [16].

**3D Shape Encoders.** An alternative to projecting shapes into 2D is to extract features directly from 3D representations. For point clouds, PointNet [2] pioneered direct point cloud processing using shared MLPs and symmetric pooling, while PointNet++ [33] introduced hierarchical feature learning to capture local geometric structures. Subsequent works improved local feature aggregation through dynamic graph convolutions (DGCNN[43]) or attention mechanisms (Point Transformer [8], PCT [13]). Recent studies show that even simple MLP architectures (PointMLP [28]) or revisited PointNet++ variants (PointNeXt [34]) achieve competitive performance with modern training strategies. Self-supervised pretraining methods such as Point-BERT [53] and Point-MAE [32] further improve transferability through masked point modeling. For voxel-based representations, 3D ShapeNets [1] and VoxNet [29] apply 3D convolutions on volumetric grids, while sparse convolutions [4] enable efficient processing of high-resolution inputs. These approaches preserve geometric information but introduce a cross-modal alignment challenge: learned 3D embeddings must be aligned with image features to enable retrieval.

**Vision-Language Pre-training.** CLIP [35] demonstrated that contrastive learning on large-scale image-text pairs yields powerful aligned representations enabling zero-shot transfer across diverse downstream tasks. CLIP employs modality-specific encoders: a Vision Transformer (ViT) [7] for images and a Transformer [42] for text. The model is trained with a symmetric cross-modal InfoNCE [31] objective that pulls matching image-text pairs together while pushing non-matching pairs apart. This paradigm has inspired extensions such as BLIP [23], SLIP [30], and FILIP [52], among others [19, 24, 54, 47, 40, 37], as well as adaptations to additional modalities [49, 48, 26, 57]. Beyond image-text retrieval, vision-language pre-training has enabled various cross-modal retrieval tasks. Composed Image Retrieval (CIR) [56] combines reference images with modification text to retrieve target images, leveraging similar contrastive objectives and pre-aligned embeddings.

**3D-Language Alignment.** Recent work extends vision-language alignment to 3D shapes. Early approaches such as PointCLIP [55] transfer CLIP’s 2D knowledge to 3D by projecting point clouds into multi-view depth maps without 3D-specific training, with PointCLIP V2 [58] improving upon this using realistic projections and GPT-generated prompts. Rather than relying on projection-based transfer, ULIP [48, 49] trains point cloud encoders to project into CLIP’s pre-aligned image-text embedding space using triplets of rendered images, text descriptions, and point clouds. By freezing the pre-trained CLIP [35] encoders and learning only the 3D branch, ULIP [48] efficiently leverages existing vision-language alignment. OpenShape [26] scales this approach to larger datasets including Objaverse [6], while Uni3D [57] further explores unified 3D representations at scale. Point-Bind [14] extends this paradigm to additional modalities including audio, and Cap3D [27] contributes a scalable automatic 3D captioning pipeline for generating large-scale training data. While these embeddings theoretically enable IBSR, prior work focused solely on zero-shot classification. Unlike multi-view methods [39, 25, 16] requiring rendered 2D representations, we leverage pre-aligned point cloud encoders directly, preserving native 3D geometry. Furthermore, we investigate how hard contrastive learning [36], which has proven effective in other metric learning contexts but has not been applied to multi-modal IBSR, can enhance instance-level discrimination in this setting. Current multi-modal 3D models typically rely on the symmetric InfoNCE loss [31], which treats all negatives within a mini-batch as equally informative. We extend the theoretical framework of Robinson et al. [36]—originally designed for single-modality contrastive learning—to the multi-modal retrieval domain. Unlike previous works that focus on class-level alignment for classification, our HCL is specifically formulated to handle the cross-modal instance-level discrimination required for high-fidelity shape retrieval.

### 3 Methodology

Image-based shape retrieval (IBSR) retrieves 3D shapes from a query image, evaluated at instance or class level. Unlike multi-view methods [51, 10, 38], we leverage pre-aligned encoders from ULIP [48, 49] and OpenShape [26], enabling compact representations and zero-shot cross-domain retrieval without retraining. We further enhance performance through fine-tuning with hard-contrastive learning [36] shown in Fig. 2 which illustrates how hard negative sampling yields near-anchor negatives that force finer discrimination and improve robustness, whereas random sampling sometimes produces easy or false negatives that degrade learning.

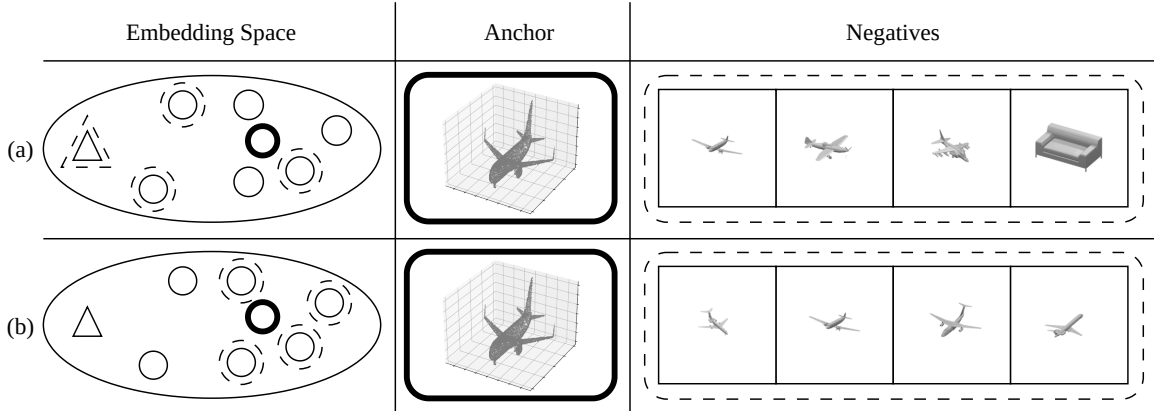


Figure 2: Comparison of (a) random sampling vs. (b) hard negative sampling [36]. Random sampling may yield out-of-class samples (e.g., couch  $\triangle$  vs. airplane  $\circ$ ), producing overly easy negatives or even false negatives (a), while hard negative sampling ensures true hard negatives close to the anchor  $\circ$  (b) (inspired by Fig. 1 of [36]).

### 3.1 IBSR Pipeline

Our pipeline (Fig. 1) consists of three components: an image encoder  $f_I$ , a point cloud encoder  $f_P$ , and a  $k$ -nearest neighbors ( $k$ -nn) matcher. Both encoders map inputs to a shared embedding space where corresponding image-shape pairs are closely positioned. Given a shape database  $D_S$ , we embed all point clouds via  $f_P$ , build a  $k$ -nn index [5], then retrieve the  $k$  nearest shapes for a query image embedded by  $f_I$ . When  $f_P$  has not seen  $D_S$  during training, this constitutes zero-shot retrieval. Following ULIP [48, 49] and OpenShape [26], we use frozen pre-aligned image-text encoders (e.g., OpenCLIP [3]) and align only the point cloud encoder, simplifying training and avoiding forgetting.

### 3.2 Design Choices

Our approach differs from prior work [51, 10, 38] in two key aspects:

**Point cloud representation.** Unlike multi-view methods [39, 22, 18], point clouds preserve explicit geometric information without requiring fusion of multiple feature tensors. This reduces data complexity (e.g., 60k values vs. 1.5M for 10-view representations) while improving robustness to rotation and partial observations. Furthermore, avoiding the need for view synthesis avoids the dependence on the number and configurations of considered views.

**Pre-aligned encoders.** We consider pre-alignment as a specific form of pre-training whose objective is to embed heterogeneous modalities into a shared latent space while enforcing cross-modal alignment. By leveraging encoders aligned on large-scale data (e.g., LAION-5B [37]), we improve data efficiency and enable zero-shot and cross-domain retrieval without retraining.

### 3.3 Image-based shape retrieval training

Pre-aligned encoders enable zero-shot retrieval on unseen shape datasets. To improve performance on domain-specific data, we tune the point cloud encoder while keeping the image encoder frozen—referred to as *standard retrieval*. Since our task involves only shapes and images, we exclude the text modality.

**Tuple Creation** fine-tuning requires point clouds paired with  $M$  rendered images per shape, yielding  $N$  point clouds with  $M$  images each ( $N:M$ ).

**Point cloud generation.** We uniformly sample  $P$  points ( $P=8,000$  for ULIP [48],  $P=10,000$  for ULIP2 [49] and OpenShape [26]) from each 3D surface. RGB values are included when available ( $P \times 6$ ), as color improves performance [26]; otherwise, uniform color is applied. Point clouds are normalized and axis-aligned with the pre-trained encoder. We apply the following augmentations: random dropout, scaling, point shift, perturbation, and rotation.

**Image generation.** We consider RGB images with the dimensions  $H \times W \times C$ . When not available, we render 12 views per shape ( $30^\circ$  elevation,  $30^\circ$  azimuth intervals) following [26, 48]. Images are preprocessed (resizing, center cropping, normalization) per downstream encoder, using OpenCLIP [3] by default. We do not apply further augmentation. For further details, we refer to the supplementary material. These images serve only for tuple creation, not shape description.

**Training framework** We finetune only the point cloud encoder  $f_P$  while keeping  $f_I$  frozen. Training follows the same contrastive objective as pre-training. Mini-batches of  $N$  shape-image tuples  $\{(p, im)\}^{1, \dots, N}$  are constructed

by augmenting each point cloud and randomly selecting one corresponding image. Embeddings from  $f_P$  and  $f_I$  are  $\ell_2$ -normalized and aligned via the multi-modal InfoNCE loss [31]:

$$\mathcal{L}_{P \rightarrow I}(\{(p, im)^N\}) = \frac{1}{N} \sum_{i=1}^N -\frac{1}{2} \log \frac{\exp(f_P(p_i)^\top f_I(im_i)/\tau)}{\sum_{j=1}^N \exp(f_P(p_i)^\top f_I(i_j)/\tau)} - \frac{1}{2} \log \frac{\exp(f_P(p_i)^\top f_I(im_i)/\tau)}{\sum_{j=1}^N \exp(f_P(p_j)^\top f_I(im_i)/\tau)} \quad (1)$$

The temperature  $\tau$  from Eq. 1 is re-initialized rather than inherited from pre-training. Since  $f_I$  is frozen, image embeddings are computed offline, significantly accelerating training.

**Hard negative learning** Standard contrastive learning samples negatives uniformly, risking uninformative gradients from easy negatives far from the anchor. We integrate hard negative sampling [36] with the multi-modal version of InfoNCE introduced by CLIP [35], using a parameterized distribution  $q$  that up-weights negatives close to positive anchors (Fig. 2). This improves instance-level discrimination without additional computational cost, as reweighting occurs within existing mini-batches. Following Robinsom et. al. [36], we modify the InfoNCE loss over a batch of positive pairs  $\{x, x^+\}$  to train a parameterized encoder  $f_\theta$  by replacing in-batch negatives with negatives sampled from distribution  $q$  denoting the distribution of true negatives. Replacing uniform sampling with  $Q$  negatives drawn from  $q$ , the objective becomes:

$$\mathcal{L}(\{x, x^+\}^N) = -\frac{1}{N} \sum_{i=1}^N \log \frac{\exp f_\theta(x_i)^\top f_\theta(x_i^+)}{\exp f_\theta(x_i)^\top f_\theta(x_i^+) + Q \mathbb{E}_{x^- \sim q_\beta} [\exp f_\theta(x_i)^\top f_\theta(x^-)]} \quad (2)$$

The novelty of our HCL (Eq.3) is the symmetric cross-modal extension. In the IBSR context, a 'hard negative' is not just a similar image, but a 3D shape whose geometric embedding is deceptively close to the query image's visual embedding. Since the context of instance level retrieval omits the necessity to take care about false-negatives In Eq. 2, all samples from  $q$  are true-negatives:  $q_\beta^-(x^-) = q_\beta(x^-)$  (Eq. 4). Extending to the multi-modal setting yields our hard contrastive loss (HCL) objective:

$$\mathcal{L}_{P \rightarrow I}^{HCL}(\{(p, im)^N\}) = \frac{1}{N} \sum_{i=1}^N \left( -\frac{1}{2} \log \frac{\exp(f_P(p_i)^\top f_I(im_i)/\tau)}{\exp(f_P(p_i)^\top f_I(im_i)/\tau) + Q \mathbb{E}_{im^- \sim q_\beta^{im}} [\exp(f_P(p_i)^\top f_I(im^-)/\tau)]} - \frac{1}{2} \log \frac{\exp(f_P(p_i)^\top f_I(im_i)/\tau)}{\exp(f_P(p_i)^\top f_I(im_i)/\tau) + Q \mathbb{E}_{p^- \sim q_\beta^p} [\exp(f_P(p^-)^\top f_I(im_i)/\tau)]} \right) \quad (3)$$

where  $\tau$  is the learnable temperature and  $Q = N - 1$  is the number of negatives per batch of size  $N$ .

**Modeling the negative distribution.** By modeling the negative distributions  $q_i^\beta$  (images) and  $q_p^\beta$  (point clouds) separately (see Eq. 4), we force the model to resolve fine-grained ambiguities that are often ignored by standard multi-modal InfoNCE [35]. The distribution  $q_\beta$  must lie on the latent hypersphere, concentrate around the anchor, and allow smoothness control via  $\beta$ . Following Robinsom et al. [36], we model  $q_\beta$  as an unnormalized von Mises-Fisher distribution using the anchor as mean direction and  $\beta$  as concentration:

$$q_\beta(x^-) \propto \exp(\beta f(x)^\top f(x^-)) \cdot p(x^-) \quad (4)$$

Fig. 3 illustrates how  $\beta$  controls the concentration of negatives around the anchor. Further details are provided in the supplementary material.

## 4 Evaluation

In order to demonstrate the potential of our approach, we compare with different baseline approaches.

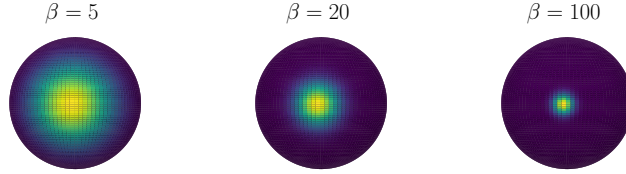


Figure 3: Von Mises-Fisher distribution on a unit hypersphere for varying  $\beta$ . Higher  $\beta$  increases concentration of  $q_\beta$  and negative hardness.

#### 4.1 Baseline techniques used for comparison

We compare against state-of-the-art methods, including ULIP [48], ULIP2 [49], and OpenShape [26], using compatible encoders and datasets. Our results demonstrate that hard contrastive learning yields comparable or improved zero-shot retrieval with pre-aligned models, while standard retrieval with Point-BERT [53] shows notable accuracy gains from our hard contrastive learning objective training (Tables 3,4,5).

#### 4.2 Metrics

We report Top- $k$  accuracy ( $Acc_{Topk}$ ) and mean average precision ( $mAP@10$ ).  $Acc_{Top1}$  measures whether the correct shape is retrieved at rank 1, while  $Acc_{Top10}$  captures whether it appears within the top 10 results. These metrics indicate retrieval success but not ranking quality. To address this,  $mAP@10$  evaluates precision across ranks, providing a complementary assessment of retrieval effectiveness. CompCars [50] and StanfordCars [21] are single class datasets, hence we report only instance level results. For all other datasets, we provide both instance-level and class-level scores. Standard retrieval results for the Pix3D [41] dataset do not present class-level scores in some cases (Tab. 4), because baseline frameworks do not evaluate them; as a result, we cannot provide retrieval-gain comparisons.

#### 4.3 Datasets

We evaluate on two dataset categories: *shape-centered* collections with train/test splits by shape, and *image-centered* IBSR benchmarks with splits by image (allowing shape overlap between splits). For shape-centered evaluation, we use ModelNet40 [46] and the LVIS [15]-annotated subset of Objaverse [6] dataset following ULIP2 [49] and OpenShape [26] protocols. For IBSR, we evaluate on Pix3D [41], CompCars [50], and StanfordCars [21]. Table 1 summarizes dataset statistics. We evaluate two Point-BERT [53] variants: Point-BERT(S) (5.1M params) and Point-BERT(L) (72.1M params).

#### 4.4 Implementation details

All experiments were conducted on 2 NVIDIA A100 GPUs using AdamW. Learning rates are  $5 \times 10^{-4}$  for Point-BERT [53] and  $1 \times 10^{-3}$  for SparseConv [4] encoders.

**Standard retrieval.** Models are finetuned using the train split with hard contrastive or InfoNCE loss. We train for 100 epochs on ModelNet40 [46] and 1000 epochs on other datasets. **Zero-shot retrieval.** Models are trained for 100 epochs on ShapeNet [1] with batch size 200, following OpenShape [26]. For the HCL, we use initial  $\beta = 0.5$  with five-stage annealing [36].

#### 4.5 Training modalities

We employ two different training modalities: Standard and zero-shot retrieval. *Zero-shot retrieval* is defined as the ability of our pre-aligned image and point-cloud encoders—aligned via large-scale image–shape pairs following PointCLIP [55] and ULIP [48]—to retrieve 3D shapes for novel image queries, including entirely unseen shape datasets, without any further training. To evaluate zero-shot performance, we apply these fixed encoders to the retrieval task. For *standard retrieval*, we freeze the image encoder and fine-tune only the shape encoder on domain-specific shapes and rendered images to adapt to the target domain. The point-cloud encoder alignment itself proceeds in two stages: (1) a pre-alignment (pre-training) phase that generally brings the point-cloud encoder into correspondence with the image encoder, and (2) a domain-specific fine-tuning phase that specializes it on the target data. Hard-negative learning (Eq. 3) is applied during both stages analyzing its effect on both *zero-shot* and *standard* retrieval modalities.

| Type           | Dataset            | Shapes | Train Img | Test Img |
|----------------|--------------------|--------|-----------|----------|
| Shape-centered | ModelNet40 [46]    | 12,311 | –         | –        |
|                | Objaverse-LVIS [6] | 46k    | –         | –        |
| Image-centered | Pix3D [41]         | 322    | 2,648     | 2,470    |
|                | CompCars [50]      | 94     | 3,798     | 1,898    |
|                | StanfordCars [21]  | 134    | 8,144     | 8,041    |

Table 1: Dataset statistics.

#### 4.6 Zero-Shot Retrieval with InfoNCE Baseline

We evaluate zero-shot retrieval on ModelNet40 [46] and Objaverse-LVIS [6]. As shown in Table 2, OpenShape [26] models consistently outperform ULIP [48, 49] for IBSR. Performance improves with (1) large-scale pre-training (Ensembled vs. ShapeNet [1]-only) and (2) increased model capacity. Point-BERT(L) [53] trained via OpenShape [26] achieves the best results. Notably, all models perform significantly better at class-level than instance-level retrieval, except SparseConv [26], which shows comparable discrimination at both levels despite lower overall accuracy. For Objaverse-LVIS evaluation, models trained on the full Ensembled dataset are excluded due to data overlap. Point-BERT(S) [53] trained on (excluding the LVIS [15] subset) achieves the best results, outperforming its ModelNet40 [46] performance by  $\sim 16\%$ —likely due to exposure to similar Objaverse [6] data during pre-training. Evaluation

| Dataset           | Framework      | Model              | Pre-train Data          | $Acc_{Top1}$     | $Acc_{Top10}$    | $mAP@10$         |
|-------------------|----------------|--------------------|-------------------------|------------------|------------------|------------------|
| Modelnet40 [46]   | ULIP [48]      | Point-BERT [53]    | Shapenet [1]            | 0.3/9.5          | 2.1/35.9         | 0.7/15.6         |
|                   |                |                    | Ensembled [26]          | 1.6/22.8         | 6.4/61.1         | 2.9/30.3         |
|                   | OpenShape [26] | Point-BERT(S) [53] | Shapenet [1]            | 18.7/71.1        | 55.2/90.7        | 29.1/73.9        |
|                   |                |                    | Ensembled [26]          | <b>30.5/97.2</b> | <b>67.1/92.9</b> | <b>41.6/80.1</b> |
|                   |                |                    | Shapenet [1]            | 9.5/63.8         | 38.0/88.2        | 17.1/67.4        |
|                   |                |                    | Ensembled [26]          | 17.9/18.0        | 51.0/52.6        | 27.6/27.7        |
|                   | ULIP2 [49]     | Point-BERT [53]    | Ensembled [26]          | 3.0/3.1          | 9.0/10.2         | 4.6/4.9          |
|                   |                |                    | Ensembled [26]          | 3.5/3.6          | 14.6/16.0        | 6.2/6.6          |
| ObjaverseLVIS [6] | ULIP [48]      | Point-BERT [53]    | Shapenet [1]            | 0.1/2.1          | 0.4/10.6         | 0.2/4.1          |
|                   | OpenShape [26] | Point-BERT(S) [53] | Shapenet [1]            | 8.2/20.7         | 26.2/49.3        | 13.2/26.3        |
|                   |                |                    | Ensembled [26] (NoLVIS) | <b>46.9/69.4</b> | <b>82.7/93.5</b> | <b>58.4/69.6</b> |
|                   |                |                    | SparseConv [4]          | Shapenet [1]     | 2.6/12.6         | 11.6/36.5        |
|                   |                |                    | Ensembled [26] (NoLVIS) | 24.7/49.6        | 60.6/84.4        | 34.9/55.0        |

Table 2: Zero-shot retrieval results for shape-centered datasets (aligned using InfoNCE loss [31]) on ModelNet40 [46], ObjaverseLVIS [6]. (Notation: *instance/class*)

| Dataset           | Framework      | Model              | Pre-train Data | $Acc_{Top1}$     | $Acc_{Top10}$    | $mAP@10$         |
|-------------------|----------------|--------------------|----------------|------------------|------------------|------------------|
| Pix3D [41]        | ULIP [48]      | Point-BERT [53]    | Shapenet [1]   | 0.4/52.5         | 3.2/80.7         | 1.0/53.9         |
|                   |                |                    | Ensembled [26] | 0.9/59.1         | 4.3/85.1         | 1.7/60.5         |
|                   | OpenShape [26] | Point-BERT(S) [53] | Shapenet [1]   | 32.8/88.5        | 81.5/98.5        | 47.6/89.1        |
|                   |                |                    | Ensembled [26] | <b>34.6/90.5</b> | <b>83.3/97.8</b> | <b>50.5/90.5</b> |
|                   |                |                    | Shapenet [1]   | 12.4/74.5        | 49.6/98.6        | 22.1/78.9        |
|                   |                |                    | Ensembled [26] | 16.4/89.9        | 61.3/99.3        | 28.5/88.5        |
|                   | ULIP2 [49]     | Point-BERT [53]    | Ensembled [26] | 0.7/57.3         | 4.2/82.1         | 1.6/60.4         |
|                   |                |                    | Ensembled [26] | 6.2/69.0         | 29.6/79.1        | 12.1/71.0        |
| CompCars [50]     | ULIP [48]      | Point-BERT [53]    | Shapenet [1]   | 0.7/-            | 10.1/-           | 2.6/-            |
|                   |                |                    | Ensembled [26] | 1.1/-            | 10.0/-           | 2.9/-            |
|                   | OpenShape [26] | Point-BERT(S) [53] | Shapenet [1]   | 10.8/-           | <b>47.7/-</b>    | <b>20.1/-</b>    |
|                   |                |                    | Ensembled [26] | <b>10.9/-</b>    | 44.2/-           | 19.5/-           |
|                   |                |                    | SparseConv [4] | 3.8/-            | 22.6/-           | 8.1/-            |
|                   | ULIP2 [49]     | Point-BERT [53]    | Ensembled [26] | 7.7/-            | 29.0/-           | 12.7/-           |
| Ensembled [26]    |                |                    | 0.7/-          | 12.8/-           | 3.2/-            |                  |
| StanfordCars [21] | ULIP [48]      | Point-BERT [53]    | Shapenet [1]   | 1.7/-            | 8.0/-            | 3.0/-            |
|                   |                |                    | Ensembled [26] | 1.8/-            | 8.6/-            | 3.3/-            |
|                   | OpenShape [26] | Point-BERT(S) [53] | Shapenet [1]   | 11.2/-           | <b>49.9/-</b>    | <b>21.9/-</b>    |
|                   |                |                    | Ensembled [26] | <b>11.4/-</b>    | 49.1/-           | 21.8/-           |
|                   |                |                    | SparseConv [4] | Shapenet [1]     | 4.0/-            | 22.1/-           |
|                   | ULIP2 [49]     | Point-BERT [53]    | Ensembled [26] | 5.6/-            | 33.1/-           | 12.2/-           |
|                   |                |                    | Ensembled [26] | 1.7/-            | 8.4/-            | 3.4/-            |
|                   |                | PointNeXt [34]     | Ensembled [26] | 0.9/-            | 12.1/-           | 3.2/-            |

Table 3: Zero-Shot retrieval results for image-centered (aligned using multi-modal InfoNCE Eq. 1) for IBSR datasets Pix3D[41], CompCars[50] and [21] (Notation: *instance/class*)

on shape-centric datasets confirms that OpenShape [26] outperforms ULIP [48, 49], with large-scale pre-training further improving zero-shot performance. The scaled Point-BERT [53] achieves sufficient class-level accuracy for retrieval-based shape classification. These trends persist on IBSR benchmarks (Table 3), where Point-BERT [53] encoders again perform best. However, zero-shot performance drops notably, particularly for instance-level retrieval. This gap stems from domain shift between synthetic pre-training data and real IBSR images. Pre-aligned models particularly struggle with instance-level retrieval compared to shape-centric datasets.

| Dataset           | Model                    | Pre-train Data | $Acc_{Top1}$     | $Acc_{Top10}$    | $mAP@10$         |
|-------------------|--------------------------|----------------|------------------|------------------|------------------|
| Modelnet40 [46]   | Point-BERT(S) [53](ours) | Shapenet [1]   | 45.1/90.2        | 88.4/98.7        | 59.3/88.3        |
|                   | Point-BERT(L) [53](ours) | Ensembled [26] | <b>57.3/92.2</b> | <b>92.5/99.1</b> | <b>69.1/88.9</b> |
|                   | SparseConv [4](ours)     | Shapenet [1]   | 42.9/89.9        | 87.1/99.1        | 57.1/88.1        |
|                   |                          | Ensembled [26] | 45.4/91.1        | 88.6/99.1        | 59.3/88.8        |
| Pix3D [41]        | LFD [12]                 | -              | 60.7/-           | 86.3/-           | -                |
|                   | HEG-TS [10]              | -              | 74.9/-           | 95.0/-           | -                |
|                   | CMIC [51]                | -              | 78.9/-           | 96.1/-           | -                |
|                   | SC-IBSR [38]             | -              | 80.2/-           | 96.9/-           | -                |
|                   | Point-BERT(S) [53](ours) | Shapenet [1]   | 77.5/97.7        | 98.5/99.9        | 85.6/93.5        |
|                   | Point-BERT(L) [53](ours) | Ensembled [26] | <b>80.7/97.7</b> | <b>98.5/99.9</b> | <b>87.8/91.1</b> |
| CompCars [50]     | SparseConv [4](ours)     | Shapenet [1]   | 71.1/97.7        | 98.3/99.9        | 81.3/94.2        |
|                   |                          | Ensembled [26] | 69.6/97.4        | 97.8/99.8        | 80.0/94.1        |
|                   | LFD [12]                 | -              | 20.5/-           | 58.0/-           | -                |
|                   | HEG-TS [10]              | -              | 67.1/-           | 93.7/-           | -                |
|                   | CMIC [51]                | -              | 77.8/-           | 94.1/-           | -                |
|                   | SC-IBSR [38]             | -              | 78.7/-           | 94.2/-           | -                |
| StanfordCars [21] | Point-BERT(S) [53](ours) | Shapenet [1]   | 93.8/-           | 99.9/-           | 96.5/-           |
|                   | Point-BERT(L) [53](ours) | Ensembled [26] | <b>97.7/-</b>    | <b>100.0/-</b>   | <b>98.8/-</b>    |
|                   | SparseConv [4](ours)     | Shapenet [1]   | 89.5/-           | 99.8/-           | 93.8/-           |
|                   |                          | Ensembled [26] | 85.1/-           | 99.2/-           | 90.5/-           |
|                   | LFD [12]                 | -              | 29.5/-           | 68.4/-           | -                |
|                   | HEG-TS [10]              | -              | 68.4/-           | 92.1/-           | -                |
| StanfordCars [21] | CMIC [51]                | -              | 83.4/-           | 96.4/-           | -                |
|                   | SC-IBSR [38]             | -              | 84.3/-           | 97.1/-           | -                |
|                   | Point-BERT(S) [53](ours) | Shapenet [1]   | 93.2/-           | 99.9/-           | 96.3/-           |
|                   | Point-BERT(L) [53](ours) | Ensembled [26] | <b>95.8/-</b>    | <b>99.9/-</b>    | <b>97.7/-</b>    |
|                   | SparseConv [4](ours)     | Shapenet [1]   | 90.5/-           | 99.9/-           | 94.7/-           |
|                   |                          | Ensembled [26] | 88.4/-           | 99.9/-           | 93.6/-           |

Table 4: Retrieval results for OpenShape [26] models finetuned with multi-modal InfoNCE loss [31] on ModelNet [46], Pix3D [41], CompCars [50], and StanfordCars [21] (*Notation: instance/class*)

| Dataset           | Model              | $Acc_{Top1}$     |                  | $Acc_{Top10}$    |                  | $mAP@10$         |                  |
|-------------------|--------------------|------------------|------------------|------------------|------------------|------------------|------------------|
|                   |                    | Ref              | HCL(ours)        | Ref              | HCL(ours)        | Ref              | HCL(ours)        |
| Modelnet40 [46]   | Point-BERT(S) [53] | 24.7/73.2        | 24.4/72.2        | <b>62.2/91.0</b> | 61.0/91.4        | 35.8/74.5        | 35.0/73.7        |
|                   | Point-BERT(L) [53] | <b>26.3/71.6</b> | 25.6/71.0        | 61.5/90.2        | 60.1/89.7        | <b>36.6/72.8</b> | 35.8/71.6        |
|                   | SparseConv [4]     | 24.5/71.2        | <b>24.2/73.3</b> | 61.6/91.1        | <b>61.2/91.4</b> | 35.4/74.0        | <b>35.2/74.5</b> |
| Pix3D [41]        | Point-BERT(S) [53] | 27.4/84.6        | 27.8/85.9        | <b>75.6/98.5</b> | 73.9/98.5        | 43.4/84.6        | 41.8/84.8        |
|                   | Point-BERT(L) [53] | 30.1/84.9        | 29.4/81.8        | 79.5/87.7        | 73.2/98.6        | 46.0/84.9        | 43.2/81.6        |
|                   | SparseConv [4]     | <b>30.6/83.0</b> | <b>33.5/87.3</b> | 79.3/97.7        | <b>97.0/99.2</b> | <b>45.7/83.4</b> | <b>47.8/86.4</b> |
| CompCars [50]     | Point-BERT(S) [53] | 10.6/-           | <b>14.0/-</b>    | 41.5/-           | <b>52.6/-</b>    | 18.3/-           | <b>24.4/-</b>    |
|                   | Point-BERT(L) [53] | <b>11.3/-</b>    | 11.2/-           | <b>48.8/-</b>    | 44.0/-           | <b>21.1/-</b>    | 19.3/-           |
|                   | SparseConv [4]     | 9.2/-            | 9.0/-            | 39.1/-           | 43.1/-           | 17.3/-           | 17.6/-           |
| StanfordCars [21] | Point-BERT(S) [53] | 11.5/-           | 10.5/-           | 45.1/-           | 43.9/-           | 20.2/-           | 19.0/-           |
|                   | Point-BERT(L) [53] | <b>12.2/-</b>    | <b>10.8/-</b>    | <b>45.9/-</b>    | 43.4/-           | <b>21.2/-</b>    | <b>19.6/-</b>    |
|                   | SparseConv [4]     | 9.6/-            | 9.0/-            | 44.0/-           | <b>44.4/-</b>    | 18.6/-           | 18.0/-           |

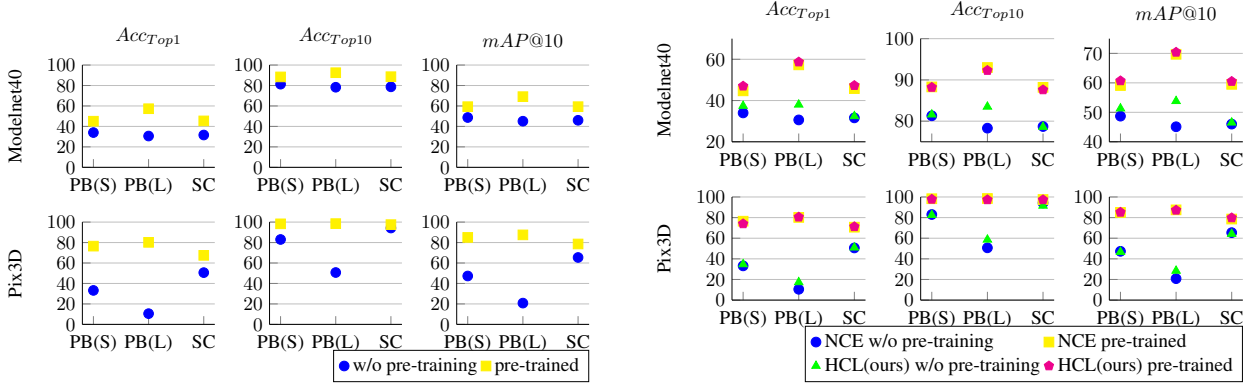
Table 5: Zero-shot retrieval on ModelNet40 [46], Pix3D [41], CompCars [50], and StanfordCars [21], trained on ShapeNet [1]. InfoNCE (Ref) vs. HCL (ours). **Highlighting** the best model for each loss objective. (*Notation: instance/class*)

#### 4.7 Standard Retrieval with InfoNCE loss

Based on zero-shot results (Section 4.6), we fine-tune the four best-performing OpenShape [26] models on datasets with available train/test splits: all IBSR benchmarks and ModelNet40 [46]. Results in Table 4 enable comparison with existing IBSR methods. On ModelNet40, zero-shot performance trends persist after fine-tuning. Point-BERT(L) [53] achieves the best instance-level  $Acc_{Top1}$  (+12% over other models), though this gap narrows to 4% at  $Acc_{Top10}$ . Class-level performance saturates at  $\sim 90\%$  across all models. On IBSR benchmarks, fine-tuned models show competitive or superior performance. For Pix3D [41], only scaled Point-BERT [53] matches SOTA at  $Acc_{Top1}$ , but all models surpass existing methods at  $Acc_{Top10}$ . On CompCars [50] and StanfordCars [21], our models outperform prior work at  $Acc_{Top1}$  and nearly saturate at  $Acc_{Top10}$ .

## 4.8 Ablation Studies

**Role of Pre-Training.** To quantify the impact of pre-alignment, we train Point-BERT(S) [53], Point-BERT(L) [53] and SparseConv [4] from scratch using identical settings as Section 4.7. As shown in Fig. 4a, pre-aligned models consistently outperform their non-pre-aligned counterparts across both datasets and all metrics. The benefit is more pronounced on Pix3D [41] than ModelNet40 [46]: Point-BERT(L) [53] shows the largest gap (**80% vs. 11%**  $Acc_{Top1}$  on Pix3D [41]), while SparseConv [4] benefits least (17% difference at  $Acc_{Top1}$ , diminishing to 3% at  $Acc_{Top10}$ ). Notably, without pre-training, model performance converges—differences shrink to  $\sim 4\%$  at  $Acc_{Top1}$ —whereas pre-alignment amplifies the gap to  $\sim 12\%$ . At  $Acc_{Top10}$ , non-pre-trained models approach pre-aligned performance, suggesting pre-training primarily improves fine-grained ranking.



(a) Instance retrieval on ModelNet40 [46] and Pix3D [41] comparing pre-trained vs. non-pre-trained OpenShape [26] models: Point-BERT(S) [53], Point-BERT(L) [53], and SparseConv [4] (PB(S), PB(L), SC).

(b) Instance retrieval performance on ModelNet40 [46] and Pix3D [41]. Comparison of InfoNCE [31] vs. HCL (ours) with/without pre-training. Models: PB(S), PB(L), SC (OpenShape [26]).

Figure 4: Comparison of pre-training and loss function effects on instance retrieval.

**HCL effects on Zero-Shot performance.** To evaluate the effect of hard negative learning on zero-shot performance (see Table 5), we pre-align point-cloud [53, 4] encoders to image-encoders on ShapeNet [1] using either standard InfoNCE loss [31] (Ref) or our hard contrastive loss (HCL), keeping all other hyperparameters fixed. Models are evaluated on the same benchmarks as Section 4.6. Table 5 shows that across ModelNet40 [46], Pix3D [41], CompCars [50], and StanfordCars [21], hard-negative learning yields scores comparable to the InfoNCE loss [31] for zero-shot retrieval.

**HCL Effects on Standard Retrieval.** HCL encourages instance-level discrimination by emphasizing hard negatives close to the anchor. We compare Point-BERT(S) [53], Point-BERT(L) [53] and SparseConv [4] trained with InfoNCE [31] vs. HCL, evaluating both pre-aligned (Section 4.7) and non-pre-aligned (Section 4.8) settings. As shown in Fig. 4b, HCL never degrades performance. On Pix3D [41], effects are negligible across all configurations. On ModelNet40 [46], SparseConv [4] shows no significant change, while Point-BERT [53] models benefit notably. Without pre-alignment, Point-BERT(S) [53] improves from 34.0% to 37.4%  $Acc_{Top1}$ ; Point-BERT(L) [53] shows larger gains (**30.6%  $\rightarrow$  38.0%**). Pre-aligned models show modest improvements at  $Acc_{Top1}$  (e.g., 57.3%  $\rightarrow$  58.7% for Point-BERT(L) [53]), with similar trends for  $mAP@10$ . In summary, HCL provides consistent gains for Point-BERT [53] architectures, particularly when training from scratch.

## 4.9 Qualitative analysis

Fig. 5 shows a representative IBSR example comparing zero-shot retrieval (with encoders aligned via InfoNCE loss [31]) and standard retrieval (fine-tuned with InfoNCE [31]/HCL). The standard retrieval achieves higher  $Acc_{Top1}$  accuracy and correctly retrieves IKEA\_EKTORP\_2 sofa from [41], illustrating that fine-tuning improves  $Acc_{Top1}$  performance and yields clearer qualitative gains.

## 5 Conclusion

We presented a point cloud-based IBSR approach that preserves geometric detail while enabling effective transfer learning. Pre-aligned encoders support zero-shot retrieval and data-efficient fine-tuning. Our multi-modal HCL with

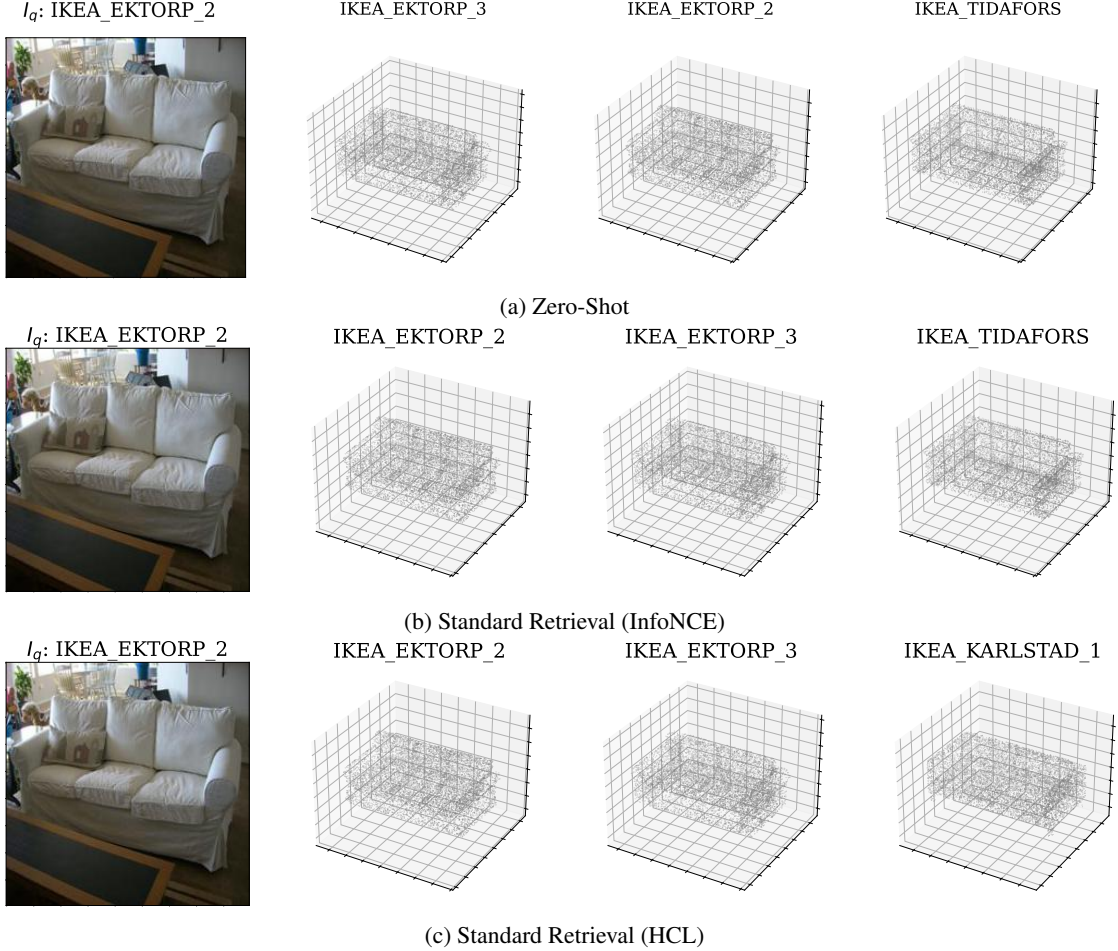


Figure 5: Qualitative results a given query image ( $I_q$ ) of the IKEA\_EKTORP\_2 sofa from [41] comparing retrieved by the scaled Point-BERT [53] model by OpenShape[26] in its pre-aligned version (a), after fine-tuning on Pix3D [41] using the InfoNCE [31] loss (b) and after fine-tuning using our multi-modal HCL loss (c).

hard negative sampling significantly improves instance-level discrimination, yielding substantial gains—particularly for Point-BERT [53] in both fine-tuning and training from scratch. Notably, our method reaches near-ceiling performance on several established benchmarks [46, 41, 50, 21], particularly in terms of  $Acc_{Top10}$ . Rather than suggesting the problem of IBSR is entirely solved, these results highlight a maturation of performance on existing datasets. This underscores the critical need for more challenging, real-world benchmarks—such as OmniObject3D [45]—to continue pushing the boundaries of instance-level 3D discrimination.

**Future work.** Current benchmarks appear near saturation, motivating more challenging datasets. Future work includes multi-task pre-alignment (pose estimation, detection, segmentation) and domain-specific validation in robotics and augmented reality.

## References

- [1] Chang, A.X., Funkhouser, T.A., Guibas, L.J., Hanrahan, P., Huang, Q., Li, Z., Savarese, S., Savva, M., Song, S., Su, H., Xiao, J., Yi, L., Yu, F.: Shapenet: An information-rich 3d model repository. CoRR **abs/1512.03012** (2015), <http://arxiv.org/abs/1512.03012>
- [2] Charles, R.Q., Su, H., Kaichun, M., Guibas, L.J.: Pointnet: Deep learning on point sets for 3d classification and segmentation. In: 2017 IEEE Conference on Computer Vision and Pattern Recognition (CVPR). pp. 77–85 (2017). <https://doi.org/10.1109/CVPR.2017.16>
- [3] Cherti, M., Beaumont, R., Wightman, R., Wortsman, M., Ilharco, G., Gordon, C., Schuhmann, C., Schmidt, L., Jitsev, J.: Reproducible scaling laws for contrastive language-image learning. In: 2023

- IEEE/CVF Conference on Computer Vision and Pattern Recognition (CVPR). pp. 2818–2829 (2023). <https://doi.org/10.1109/CVPR52729.2023.00276>
- [4] Choy, C., Gwak, J., Savarese, S.: 4d spatio-temporal convnets: Minkowski convolutional neural networks. In: 2019 IEEE/CVF Conference on Computer Vision and Pattern Recognition (CVPR). pp. 3070–3079 (2019). <https://doi.org/10.1109/CVPR.2019.00319>
- [5] Cunningham, P., Delany, S.J.: k-nearest neighbour classifiers - a tutorial. *ACM Comput. Surv.* **54**(6) (Jul 2021). <https://doi.org/10.1145/3459665>, <https://doi.org/10.1145/3459665>
- [6] Deitke, M., Schwenk, D., Salvador, J., Weihs, L., Michel, O., VanderBilt, E., Schmidt, L., Ehsani, K., Kembhavi, A., Farhadi, A.: Objaverse: A universe of annotated 3d objects. In: Proceedings of the IEEE/CVF Conference on Computer Vision and Pattern Recognition. pp. 13142–13153 (2023)
- [7] Dosovitskiy, A., Beyer, L., Kolesnikov, A., Weissenborn, D., Zhai, X., Unterthiner, T., Dehghani, M., Minderer, M., Heigold, G., Gelly, S., Uszkoreit, J., Houlsby, N.: An image is worth 16x16 words: Transformers for image recognition at scale. In: 9th International Conference on Learning Representations, ICLR 2021, Virtual Event, Austria, May 3-7, 2021. OpenReview.net (2021), <https://openreview.net/forum?id=YicbFdNTTy>
- [8] Engel, N., Belagiannis, V., Dietmayer, K.: Point transformer. *IEEE Access* **9**, 134826–134840 (2021). <https://doi.org/10.1109/ACCESS.2021.3116304>
- [9] Feng, Y., Zhang, Z., Zhao, X., Ji, R., Gao, Y.: Gvcnn: Group-view convolutional neural networks for 3d shape recognition. In: 2018 IEEE/CVF Conference on Computer Vision and Pattern Recognition. pp. 264–272 (2018). <https://doi.org/10.1109/CVPR.2018.00035>
- [10] Fu, H., Li, S., Jia, R., Gong, M., Zhao, B., Tao, D.: Hard example generation by texture synthesis for cross-domain shape similarity learning. In: Larochelle, H., Ranzato, M., Hadsell, R., Balcan, M., Lin, H. (eds.) *Advances in Neural Information Processing Systems 33: Annual Conference on Neural Information Processing Systems 2020, NeurIPS 2020, December 6-12, 2020, virtual (2020)*, <https://proceedings.neurips.cc/paper/2020/hash/a87d27f712df362cd22c7a8ef823e987-Abstract.html>
- [11] Grabner, A., Roth, P.M., Lepetit, V.: 3d pose estimation and 3d model retrieval for objects in the wild. In: 2018 IEEE Conference on Computer Vision and Pattern Recognition, CVPR 2018, Salt Lake City, UT, USA, June 18-22, 2018. pp. 3022–3031. Computer Vision Foundation / IEEE Computer Society (2018). <https://doi.org/10.1109/CVPR.2018.00319>, [http://openaccess.thecvf.com/content\\_cvpr\\_2018/html/Grabner\\_3D\\_Pose\\_Estimation\\_CVPR\\_2018\\_paper.html](http://openaccess.thecvf.com/content_cvpr_2018/html/Grabner_3D_Pose_Estimation_CVPR_2018_paper.html)
- [12] Grabner, A., Roth, P.M., Lepetit, V.: Location field descriptors: Single image 3d model retrieval in the wild. In: 2019 International Conference on 3D Vision, 3DV 2019, Québec City, QC, Canada, September 16-19, 2019. pp. 583–593. IEEE (2019). <https://doi.org/10.1109/3DV.2019.00070>, <https://doi.org/10.1109/3DV.2019.00070>
- [13] Guo, M.H., Cai, J.X., Liu, Z.N., Mu, T.J., Martin, R.R., Hu, S.M.: Pct: Point cloud transformer. *Computational Visual Media* **7**(2), 187–199 (2021). <https://doi.org/10.1007/s41095-021-0229-5>
- [14] Guo, Z., Zhang, R., Zhu, X., Tang, Y., Ma, X., Han, J., Chen, K., Gao, P., Li, X., Li, H., Heng, P.A.: Point-bind & point-llm: Aligning point cloud with multi-modality for 3d understanding, generation, and instruction following (2023), <https://arxiv.org/abs/2309.00615>
- [15] Gupta, A., Dollár, P., Girshick, R.B.: Lvis: A dataset for large vocabulary instance segmentation. 2019 IEEE/CVF Conference on Computer Vision and Pattern Recognition (CVPR) pp. 5351–5359 (2019), <https://api.semanticscholar.org/CorpusID:195441339>
- [16] Hamdi, A., Giancola, S., Ghanem, B.: Mvtn: Multi-view transformation network for 3d shape recognition. In: International Conference on Computer Vision (ICCV). pp. 1–11 (2021)
- [17] Han, X., Niu, D., Diao, Z., Zhang, C., Nie, H., Li, Y.: Single image 3d model retrieval based on feature fusion and view grouping. In: 2024 International Conference on Virtual Reality and Visualization (ICVRV). pp. 66–71 (2024). <https://doi.org/10.1109/ICVRV62410.2024.00021>
- [18] He, X., Huang, T., Bai, S., Bai, X.: View n-gram network for 3d object retrieval. In: 2019 IEEE/CVF International Conference on Computer Vision, ICCV 2019, Seoul, Korea (South), October 27 - November 2, 2019. pp. 7514–7523. IEEE (2019). <https://doi.org/10.1109/ICCV.2019.00761>, <https://doi.org/10.1109/ICCV.2019.00761>
- [19] Jia, C., Yang, Y., Xia, Y., Chen, Y.T., Parekh, Z., Pham, H., Le, Q., Sung, Y.H., Li, Z., Duerig, T.: Scaling up visual and vision-language representation learning with noisy text supervision. In: Meila, M., Zhang, T. (eds.) *Proceedings of the 38th International Conference on Machine Learning. Proceedings of Machine Learning Research*, vol. 139, pp. 4904–4916. PMLR (18–24 Jul 2021), <https://proceedings.mlr.press/v139/jia21b.html>

- [20] Kanezaki, A., Matsushita, Y., Nishida, Y.: Rotationnet: Joint object categorization and pose estimation using multiviews from unsupervised viewpoints. In: 2018 IEEE Conference on Computer Vision and Pattern Recognition, CVPR 2018, Salt Lake City, UT, USA, June 18-22, 2018. pp. 5010–5019. Computer Vision Foundation / IEEE Computer Society (2018). <https://doi.org/10.1109/CVPR.2018.00526>, [http://openaccess.thecvf.com/content\\_cvpr\\_2018/html/Kanezaki\\_RotationNet\\_Joint\\_Object\\_CVPR\\_2018\\_paper.html](http://openaccess.thecvf.com/content_cvpr_2018/html/Kanezaki_RotationNet_Joint_Object_CVPR_2018_paper.html)
- [21] Krause, J., Stark, M., Deng, J., Fei-Fei, L.: 3d object representations for fine-grained categorization. In: 2013 IEEE International Conference on Computer Vision Workshops, ICCV Workshops 2013, Sydney, Australia, December 1-8, 2013. pp. 554–561. IEEE Computer Society (2013). <https://doi.org/10.1109/ICCVW.2013.77>, <https://doi.org/10.1109/ICCVW.2013.77>
- [22] Lee, T., Lin, Y., Chiang, H., Chiu, M., Hsu, W.H., Huang, P.: Cross-domain image-based 3d shape retrieval by view sequence learning. In: 2018 International Conference on 3D Vision, 3DV 2018, Verona, Italy, September 5-8, 2018. pp. 258–266. IEEE Computer Society (2018). <https://doi.org/10.1109/3DV.2018.00038>, <https://doi.org/10.1109/3DV.2018.00038>
- [23] Li, J., Li, D., Xiong, C., Hoi, S.C.H.: BLIP: bootstrapping language-image pre-training for unified vision-language understanding and generation. In: Chaudhuri, K., Jegelka, S., Song, L., Szepesvári, C., Niu, G., Sabato, S. (eds.) International Conference on Machine Learning, ICML 2022, 17-23 July 2022, Baltimore, Maryland, USA. Proceedings of Machine Learning Research, vol. 162, pp. 12888–12900. PMLR (2022), <https://proceedings.mlr.press/v162/li22n.html>
- [24] Li, Y., Liang, F., Zhao, L., Cui, Y., Ouyang, W., Shao, J., Yu, F., Yan, J.: Supervision exists everywhere: A data efficient contrastive language-image pre-training paradigm. CoRR **abs/2110.05208** (2021), <https://arxiv.org/abs/2110.05208>
- [25] Liu, A., Hu, N., Song, D., Guo, F., Zhou, H., Hao, T.: Multi-view hierarchical fusion network for 3d object retrieval and classification. IEEE Access **7**, 153021–153030 (2019). <https://doi.org/10.1109/ACCESS.2019.2947245>, <https://doi.org/10.1109/ACCESS.2019.2947245>
- [26] Liu, M., Shi, R., Kuang, K., Zhu, Y., Li, X., Han, S., Cai, H., Porikli, F., Su, H.: Openshape: Scaling up 3d shape representation towards open-world understanding. CoRR **abs/2305.10764** (2023). <https://doi.org/10.48550/ARXIV.2305.10764>, <https://doi.org/10.48550/arXiv.2305.10764>
- [27] Luo, T., Rockwell, C., Lee, H., Johnson, J.: Scalable 3d captioning with pretrained models (2023), <https://arxiv.org/abs/2306.07279>
- [28] Ma, X., Qin, C., You, H., Ran, H., Fu, Y.: Rethinking network design and local geometry in point cloud: A simple residual mlp framework (2022), <https://arxiv.org/abs/2202.07123>
- [29] Maturana, D., Scherer, S.A.: Voxnet: A 3d convolutional neural network for real-time object recognition. In: 2015 IEEE/RSJ International Conference on Intelligent Robots and Systems, IROS 2015, Hamburg, Germany, September 28 - October 2, 2015. pp. 922–928. IEEE (2015). <https://doi.org/10.1109/IROS.2015.7353481>, <https://doi.org/10.1109/IROS.2015.7353481>
- [30] Mu, N., Kirillov, A., Wagner, D., Xie, S.: Slip: Self-supervision meets language-image pre-training. arXiv preprint arXiv:2112.12750 (2021)
- [31] van den Oord, A., Li, Y., Vinyals, O.: Representation learning with contrastive predictive coding. CoRR **abs/1807.03748** (2018), <http://arxiv.org/abs/1807.03748>
- [32] Pang, Y., Wang, W., Tay, F.E.H., Liu, W., Tian, Y., Yuan, L.: Masked autoencoders for point cloud self-supervised learning (2022), <https://arxiv.org/abs/2203.06604>
- [33] Qi, C.R., Yi, L., Su, H., Guibas, L.J.: Pointnet++: deep hierarchical feature learning on point sets in a metric space. In: Proceedings of the 31st International Conference on Neural Information Processing Systems. p. 5105–5114. NIPS’17, Curran Associates Inc., Red Hook, NY, USA (2017)
- [34] Qian, G., Li, Y., Peng, H., Mai, J., Hammoud, H.A.A.K., Elhoseiny, M., Ghanem, B.: Pointnext: Revisiting pointnet++ with improved training and scaling strategies (2022), <https://arxiv.org/abs/2206.04670>
- [35] Radford, A., Kim, J.W., Hallacy, C., Ramesh, A., Goh, G., Agarwal, S., Sastry, G., Askell, A., Mishkin, P., Clark, J., Krueger, G., Sutskever, I.: Learning transferable visual models from natural language supervision. In: Meila, M., Zhang, T. (eds.) Proceedings of the 38th International Conference on Machine Learning, ICML 2021, 18-24 July 2021, Virtual Event. Proceedings of Machine Learning Research, vol. 139, pp. 8748–8763. PMLR (2021), <http://proceedings.mlr.press/v139/radford21a.html>
- [36] Robinson, J.D., Chuang, C., Sra, S., Jegelka, S.: Contrastive learning with hard negative samples. In: 9th International Conference on Learning Representations, ICLR 2021, Virtual Event, Austria, May 3-7, 2021. OpenReview.net (2021), <https://openreview.net/forum?id=CR1XOQOUTH->

- [37] Schuhmann, C., Beaumont, R., Vencu, R., Gordon, C., Wightman, R., Cherti, M., Coombes, T., Katta, A., Mullis, C., Wortsman, M., Schramowski, P., Kundurthy, S., Crowson, K., Schmidt, L., Kaczmarczyk, R., Jitsev, J.: LAION-5B: an open large-scale dataset for training next generation image-text models. In: Koyejo, S., Mohamed, S., Agarwal, A., Belgrave, D., Cho, K., Oh, A. (eds.) *Advances in Neural Information Processing Systems 35: Annual Conference on Neural Information Processing Systems 2022, NeurIPS 2022*, New Orleans, LA, USA, November 28 - December 9, 2022 (2022), [http://papers.nips.cc/paper\\_files/paper/2022/hash/a1859debf3b59d094f3504d5ebb6c25-Abstract-Datasets\\_and\\_Benchmarks.html](http://papers.nips.cc/paper_files/paper/2022/hash/a1859debf3b59d094f3504d5ebb6c25-Abstract-Datasets_and_Benchmarks.html)
- [38] Song, D., Huo, S., Fu, X., Zhang, C., Li, W., Liu, A.A.: Cross-modal contrastive learning with a style-mixed bridge for single image 3d shape retrieval. *ACM Trans. Multimedia Comput. Commun. Appl.* **20**(12) (Nov 2024). <https://doi.org/10.1145/3689645>, <https://doi.org/10.1145/3689645>
- [39] Su, H., Maji, S., Kalogerakis, E., Learned-Miller, E.G.: Multi-view convolutional neural networks for 3d shape recognition. In: *2015 IEEE International Conference on Computer Vision, ICCV 2015*, Santiago, Chile, December 7-13, 2015. pp. 945–953. IEEE Computer Society (2015). <https://doi.org/10.1109/ICCV.2015.114>, <https://doi.org/10.1109/ICCV.2015.114>
- [40] Sun, Q., Fang, Y., Wu, L., Wang, X., Cao, Y.: Eva-clip: Improved training techniques for clip at scale (2023), <https://arxiv.org/abs/2303.15389>
- [41] Sun, X., Wu, J., Zhang, X., Zhang, Z., Zhang, C., Xue, T., Tenenbaum, J.B., Freeman, W.T.: Pix3d: Dataset and methods for single-image 3d shape modeling. In: *2018 IEEE Conference on Computer Vision and Pattern Recognition, CVPR 2018*, Salt Lake City, UT, USA, June 18-22, 2018. pp. 2974–2983. Computer Vision Foundation / IEEE Computer Society (2018). <https://doi.org/10.1109/CVPR.2018.00314>, [http://openaccess.thecvf.com/content\\_cvpr\\_2018/html/Sun\\_Pix3D\\_Dataset\\_and\\_CVPR\\_2018\\_paper.html](http://openaccess.thecvf.com/content_cvpr_2018/html/Sun_Pix3D_Dataset_and_CVPR_2018_paper.html)
- [42] Vaswani, A., Shazeer, N., Parmar, N., Uszkoreit, J., Jones, L., Gomez, A.N., Kaiser, L., Polosukhin, I.: Attention is all you need. *CoRR* **abs/1706.03762** (2017), <http://arxiv.org/abs/1706.03762>
- [43] Wang, Y., Sun, Y., Liu, Z., Sarma, S.E., Bronstein, M.M., Solomon, J.M.: Dynamic graph cnn for learning on point clouds. *ACM Trans. Graph.* **38**(5) (Oct 2019). <https://doi.org/10.1145/3326362>, <https://doi.org/10.1145/3326362>
- [44] Wei, X., Yu, R., Sun, J.: View-gcn: View-based graph convolutional network for 3d shape analysis. In: *2020 IEEE/CVF Conference on Computer Vision and Pattern Recognition (CVPR)*. pp. 1847–1856 (2020). <https://doi.org/10.1109/CVPR42600.2020.00192>
- [45] Wu, T., Zhang, J., Fu, X., Wang, Y., Jiawei Ren, L.P., Wu, W., Yang, L., Wang, J., Qian, C., Lin, D., Liu, Z.: Omniobject3d: Large-vocabulary 3d object dataset for realistic perception, reconstruction and generation. In: *IEEE/CVF Conference on Computer Vision and Pattern Recognition (CVPR) (2023)*
- [46] Wu, Z., Song, S., Khosla, A., Yu, F., Zhang, L., Tang, X., Xiao, J.: 3d shapenets: A deep representation for volumetric shapes. In: *Proceedings of the IEEE Conference on Computer Vision and Pattern Recognition (CVPR) (2015)*
- [47] Xu, H., Xie, S., Tan, X., Huang, P.Y., Howes, R., Sharma, V., Li, S.W., Ghosh, G., Zettlemoyer, L., Feichtenhofer, C.: Demystifying clip data. In: Kim, B., Yue, Y., Chaudhuri, S., Fragkiadaki, K., Khan, M., Sun, Y. (eds.) *International Conference on Learning Representations*. vol. 2024, pp. 47812–47831 (2024), [https://proceedings.iclr.cc/paper\\_files/paper/2024/file/d1450d6c10c6b6cf1b80964357f5fa08-Paper-Conference.pdf](https://proceedings.iclr.cc/paper_files/paper/2024/file/d1450d6c10c6b6cf1b80964357f5fa08-Paper-Conference.pdf)
- [48] Xue, L., Gao, M., Xing, C., Martín-Martín, R., Wu, J., Xiong, C., Xu, R., Niebles, J.C., Savarese, S.: Ulip: Learning a unified representation of language, images, and point clouds for 3d understanding (2023), <https://arxiv.org/abs/2212.05171>
- [49] Xue, L., Yu, N., Zhang, S., Panagopoulou, A., Li, J., Martín-Martín, R., Wu, J., Xiong, C., Xu, R., Niebles, J.C., Savarese, S.: Ulip-2: Towards scalable multimodal pre-training for 3d understanding. In: *2024 IEEE/CVF Conference on Computer Vision and Pattern Recognition (CVPR)*. pp. 27081–27091 (2024). <https://doi.org/10.1109/CVPR52733.2024.02558>
- [50] Yang, L., Luo, P., Loy, C.C., Tang, X.: A large-scale car dataset for fine-grained categorization and verification. In: *IEEE Conference on Computer Vision and Pattern Recognition, CVPR 2015*, Boston, MA, USA, June 7-12, 2015. pp. 3973–3981. IEEE Computer Society (2015). <https://doi.org/10.1109/CVPR.2015.7299023>, <https://doi.org/10.1109/CVPR.2015.7299023>
- [51] Yang, M.X., Wang, J., Lai, H., Jia, Y.K., Zhao, R., Gao, B.: Single image 3d shape retrieval via cross-modal instance and category contrastive learning. In: *International Conference on Computer Vision (ICCV) (2021)*

- [52] Yao, L., Huang, R., Hou, L., Lu, G., Niu, M., Xu, H., Liang, X., Li, Z., Jiang, X., Xu, C.: FILIP: fine-grained interactive language-image pre-training. In: The Tenth International Conference on Learning Representations, ICLR 2022, Virtual Event, April 25-29, 2022. OpenReview.net (2022), <https://openreview.net/forum?id=cpDhcsEDC2>
- [53] Yu, X., Tang, L., Rao, Y., Huang, T., Zhou, J., Lu, J.: Point-bert: Pre-training 3d point cloud transformers with masked point modeling. In: Proceedings of the IEEE Conference on Computer Vision and Pattern Recognition (CVPR) (2022)
- [54] Zhai, X., Mustafa, B., Kolesnikov, A., Beyer, L.: Sigmoid loss for language image pre-training. In: 2023 IEEE/CVF International Conference on Computer Vision (ICCV). pp. 11941–11952 (2023). <https://doi.org/10.1109/ICCV51070.2023.01100>
- [55] Zhang, R., Guo, Z., Zhang, W., Li, K., Miao, X., Cui, B., Qiao, Y., Gao, P., Li, H.: Pointclip: Point cloud understanding by CLIP. In: IEEE/CVF Conference on Computer Vision and Pattern Recognition, CVPR 2022, New Orleans, LA, USA, June 18-24, 2022. pp. 8542–8552. IEEE (2022). <https://doi.org/10.1109/CVPR52688.2022.00836>, <https://doi.org/10.1109/CVPR52688.2022.00836>
- [56] Zheng, L., Yang, Y., Tian, Q.: SIFT meets CNN: A decade survey of instance retrieval. *IEEE Trans. Pattern Anal. Mach. Intell.* **40**(5), 1224–1244 (2018). <https://doi.org/10.1109/TPAMI.2017.2709749>, <https://doi.org/10.1109/TPAMI.2017.2709749>
- [57] Zhou, J., Wang, J., Ma, B., Liu, Y.S., Huang, T., Wang, X.: Uni3d: Exploring unified 3d representation at scale. In: International Conference on Learning Representations (ICLR) (2024)
- [58] Zhu, X., Zhang, R., He, B., Guo, Z., Zeng, Z., Qin, Z., Zhang, S., Gao, P.: Pointclip v2: Prompting clip and gpt for powerful 3d open-world learning (2023), <https://arxiv.org/abs/2211.11682>